Charge puddles complicate nonlinear transport in large Berry phase materials

Arya Thenapparambil,[1,2,3] Kajetan M. Fijalkowski,[1,3,*] Mohamed AbdelGhany,[1,3] Hartmut Buhmann,[1,3] Charles Gould,[1,3,†] and Laurens W. Molenkamp[1,2,3]

[1]*Faculty for Physics and Astronomy (EP3), Universität Würzburg, Am Hubland, D-97074 Würzburg, Germany*
[2]*Max Planck Institute for Chemical Physics of Solids, Nöthnitzer Straße 40, D-01187 Dresden, Germany*
[3]*Institute for Topological Insulators, Am Hubland, D-97074 Würzburg, Germany*

(Received 15 October 2025; revised 26 January 2026; accepted 5 February 2026; published 3 March 2026)

Nonlinear transport in narrow band-gap materials has recently attracted significant attention, being commonly recognized as a useful tool to study a variety of complex physical effects related to Berry phase. Here we demonstrate that a mundane, commonly overlooked mechanism stemming from tunneling between charge puddles, can drive substantial nonlinearities in these narrow band gap materials. As a test bed, we use an epitaxial topological HgTe layer, underscoring that even good crystalline quality materials suffer from this issue. Indeed, we show that signatures of electrical transport through a network of charge puddles are not limited to the *linear* planar magnetoresistance, but also dominate *nonlinear* transport. Our findings highlight the need for utmost caution when interpreting nonlinear electrical transport phenomena, as harmonic distortion of the electrical signal, caused by charge puddles, is unavoidable in any realistic narrow-gap system, complicating the identification of other proposed effects related to the Berry phase.

DOI: 10.1103/mc1p-blhk

I. INTRODUCTION

It has long been understood that the concept of Berry phase [1,2] is fundamental to the electronic properties of a crystal, a notion that turns out to be extraordinarily useful, among others, for a description of various Hall effects [2–6] and topological phenomena [2,7]. Moreover, the effects go beyond the linear response regime, as the combination of Berry curvature and a nonequilibrium distribution of current carrying electrons can produce a net Hall signal in the second order response, even in some time-reversal invariant materials [8]. The notion that studies of nonlinear electrical transport can provide direct experimental access to subtle band structure properties, prompted substantial follow-up research effort in this direction [9–20].

Importantly, such nonlinearities are generally small in magnitude, producing subpercent corrections to the linear transport. This implies that their study requires great care to separate them from other, even mundane sources of nonlinearities, necessitating extraordinarily thorough electrical circuit considerations. Also, Berry phase invariably is tied to small band gaps in the relevant material systems. As such, another, potential trivial source of nonlinearity to which such materials will be susceptible, is spatial inhomogeneities in the device [21–24], which result in the formation of density fluctuations and charge puddles. At finite bias, charge transport between the puddles occurs via tunneling, which is an inherently nonlinear process.

We recently explored the effects of such inhomogeneities in the *linear* response magnetotransport of topological surface states [25]. We found a complex dependence on in-plane magnetic fields that is rich in structure, and can be completely understood by considering two key factors: the tilting of the Dirac cone induced by the in-plane magnetic field, which accounts for anisotropic magnetoresistance and planar Hall effect [26], and the occurrence of super-resonant tunneling of electrons facilitated by a network of charge puddles. In this paper, we explore the *nonlinear* response to the electric bias and find that these charge puddles also lead to harmonic distortion of the electrical signal, which can produce rich nonlinear corrections to the conductivity of at least comparable amplitude to that of predicted novel band structure related effects. Thus, our observations imply that great caution is needed when analyzing nonlinear transport phenomena, especially in narrow band-gap materials.

II. CHARGE PUDDLES DOMINATE THE NONLINEAR TRANSPORT

Our experimental platform is based on strained HgTe layers grown by molecular beam epitaxy [27]. Strain control is achieved by growing the 94-nm-thick HgTe layer on a CdTe-$Cd_{0.5}Zn_{0.5}Te$ superlattice. This imposes a compressive strain of 0.26% on the HgTe layer. This strain lifts the degeneracy of the two touching Γ_8 bands at the Γ point, forming linear crossing points in the band structure that exhibit Weyl semimetal behavior in the bulk [28]. However, the topological

*Contact author: kajetan.fijalkowski@uni-wuerzburg.de
†Contact author: gould@uni-wuerzburg.de

Published by the American Physical Society under the terms of the Creative Commons Attribution 4.0 International license. Further distribution of this work must maintain attribution to the author(s) and the published article's title, journal citation, and DOI.

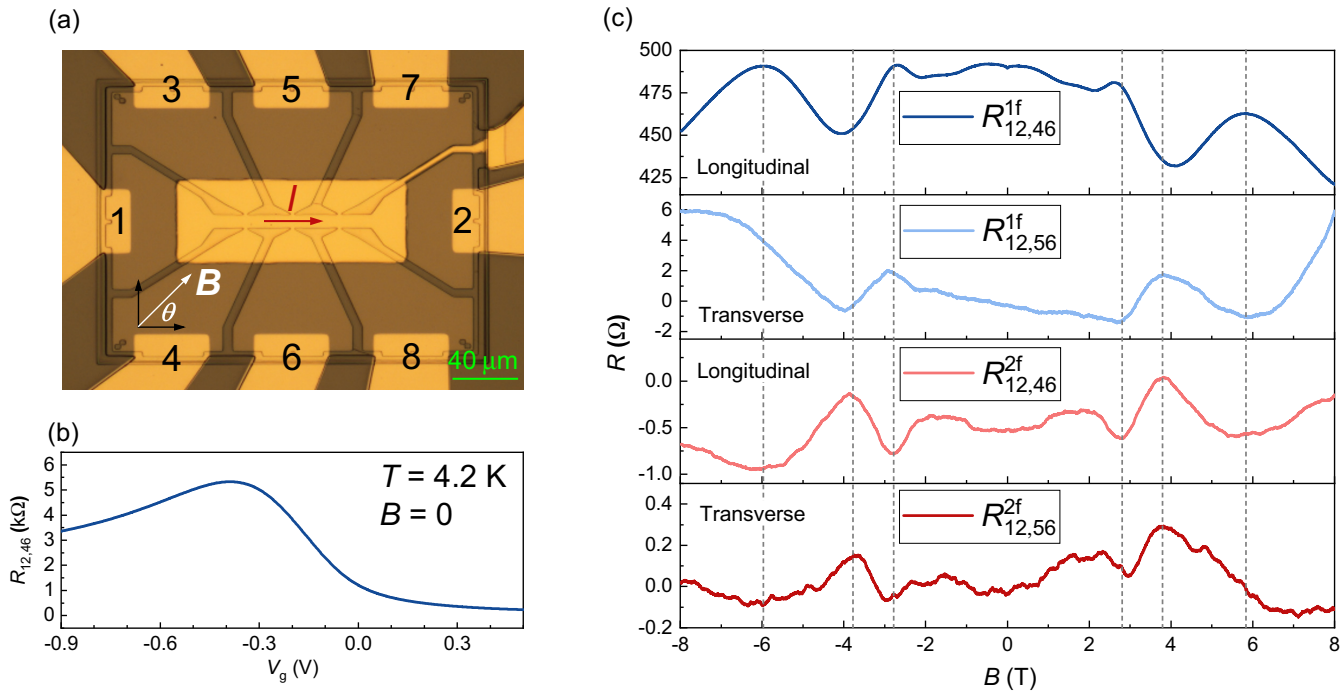


FIG. 1. (a) Optical microscopy image of the eight-terminal Hall bar showing the contact layout and the direction of the current and magnetic field. The angle θ denotes the in-plane angle between the current direction and magnetic field, with $\theta = 0°$ corresponding to the configuration where both are parallel. The current flows along the [110] crystallographic direction. (b) Gate voltage dependence of the $1f$ longitudinal resistance of the device at zero magnetic field. (c) The four-probe resistances $R^{1f}_{12,46}(B)$, $R^{1f}_{12,56}(B)$ (after subtraction of a linear contribution; see text for details), $R^{2f}_{12,46}(B)$, and $R^{2f}_{12,56}(B)$ as functions of in-plane magnetic field applied parallel to the current direction are shown in the four panels, respectively. The data in (c) are taken at a representative gate voltage of 0.2 V in the surface states (see Supplemental Material for additional gate voltages [32]). The vertical dashed lines are guides to the eye.

surface states formed by the inverted band ordering of the Γ_6 and Γ_8 bands persist and dominate the transport at higher carrier densities [29]. This allows us to controllably adjust the Fermi level to regimes of surface state or bulk Weyl node-dominated transport using a gate electrode, which makes our observations apply to a broad range of experiments described in the literature.

This layer stack is patterned into an eight-terminal Hall bar geometry (30 μm × 10 μm) using optical lithography and wet etching techniques [30]. The device includes a 5 nm Ti/100 nm Au gate electrode with a 14-nm-thick HfO_2 dielectric layer grown by atomic layer deposition at room temperature [31]. Ohmic contacts are made from 50 nm/50 nm AuGe/Au layers. A microscope image of the Hall bar with contact layout is given in Fig. 1(a).

All measurements are done at 4.2 K in a ^{4}He cryostat equipped with an 8 T magnet. Variation of the angle of the external magnetic field relative to the sample is achieved by mechanical rotation of the sample. Resistances are measured in a four-probe configuration using low-frequency ac lock-in techniques and an ultralow distortion function generator [34] as an excitation source. Second harmonic voltages are detected at double frequency ($2f$), and with a phase shift of 90° to the sinusoidal excitation, using multistage filtering. We refer to Supplemental Material for a detailed circuit diagram and a discussion of the detection method [32,33].

Figure 1(b) shows the zero-field longitudinal resistance of the device as a function of gate voltage V_g, which tunes the position of the Fermi level. The studied gate voltage range spans from surface state–dominated highly doped n-type (1.8×10^{12} cm^{-2}) conductance at 0.5 V to strong p-type (-1×10^{12} cm^{-2}) conductance at -0.9 V. The resistance maximum at -0.39 V is associated with the Fermi level being at the Weyl points [29].

For all measurements reported in this paper, we use the notation $R_{ij,kl}$ to indicate the ratio of a voltage detected between contact k and l, in response to a current flowing from contact i to j. The superscript $1f$ ($2f$) indicates that the voltage is detected as the same (double the) frequency of the current. In the top two panels of Fig. 1(c), we show standard measurements of the longitudinal and transverse resistance of the Hall bar. A 37.2 Hz ac current is passed from contact 1 to 2 (bias voltage of a few millivolts), and the same frequency ($1f$) voltage response is measured between contacts 4 and 6 to extract $R_{12,46}$ (longitudinal resistance) or between contacts 5 and 6 for $R_{12,56}$ (transverse resistance). A linear slope in B has been subtracted from $R_{12,56}$, to remove the classical Hall resistance, to account for a slight misalignment of the sample (less than 3°) relative to the magnet axis (see Supplemental Material for raw data [32]). As a function of a magnetic field applied parallel to the current, both $R_{12,46}$ and $R_{12,56}$ show strong aperiodic fluctuations. The nonzero $R_{12,56}$, which is unexpected for the planar Hall effect in this configuration arises due to an admixture of $R_{12,46}$ in $R_{12,56}$.

As previously established, both these observations are the result of an inhomogeneous current distribution arising from

charge puddles [25]. Such a distribution of puddles forms a random network of potential barriers in the device (barriers of various height separating various puddles). Each puddle by itself causes pronounced fluctuations in magnetoconductance due to lateral super-resonant tunneling to its neighbors [35]. Our device, given the size scales (puddles of diameter of some 100 nm, with a typical separation of 1 μm [23]), contains multiple randomly distributed puddles, and the joint transport through the network produces the observed aperiodic fluctuations [25].

In the lower two panels of the figure, we adjust the lock-ins to detect the $2f$ (i.e., double the frequency of the ac current) component of the same two voltages, in order to focus in on the nonlinear response. For quantitative comparison to the $1f$ signals (to keep the same units, ohm), voltage amplitude of the measured $2f$ signal is divided by the $1f$ bias current amplitude (see Supplemental Material for more details [32]). The vertical dashed lines are guides to the eye.

As expected, the amplitude of the $2f$ signal changes quadratically with bias (at low enough bias, before higher order corrections become relevant; see Supplemental Material [32]). The sample response is frequency independent. This is also expected as any ac measurement in the low-frequency regime serves merely to improve the experimental resolution, whereas the fundamental observable is the I-V characteristic of the device.

Similarly to the $1f$ case, the $2f$ signals in Fig. 1 show strong aperiodic fluctuations. Notably, the extrema in the $2f$ signal align well with those in the $1f$ response, suggesting a shared underlying mechanism. This correlation can be understood because the tunneling mechanism of transport between the puddles [25] is inherently nonlinear. Even the slightest nonlinearity implies that the response to a perfectly sinusoidal excitation will be a distorted sine wave. The Fourier expansion of such a wave contains not only the fundamental frequency, but also higher harmonics (see Supplemental Material for derivation [32]), resulting in a so-called harmonic distortion of the signal [36].

To further emphasize that these $2f$ signals depend primarily on a local puddle configuration near the contact, rather than being a valid measurement of any universal bulk property of the material, in Fig. 2 we present transverse resistance measurements on each of the pairs of contacts, as a function of a magnetic field, here applied parallel to the current. If the signal results from novel Hall transport effects intrinsic to the band structure of the material, then obviously the same signal should be observed at each pair of leads. As seen in Fig. 2, the reality is markedly different. Indeed, for the most part, there is little correlation between the three signals, to the point that at some gate voltages, the primary sign of the transverse signal depends on the choice of a contact pair. Also, the positions of extrema in the curves differ between various contact pairs. This is expected, as the magnetic field values at which they occur depend on the exact local configuration of charge puddles near each contact pair.

We also note that the presence of random inhomogeneities in the material (such as charge puddles) inherently results in a local admixing of resistivity tensor elements, randomly combining the symmetric (longitudinal) and antisymmetric (transverse) responses to an external magnetic field. This is

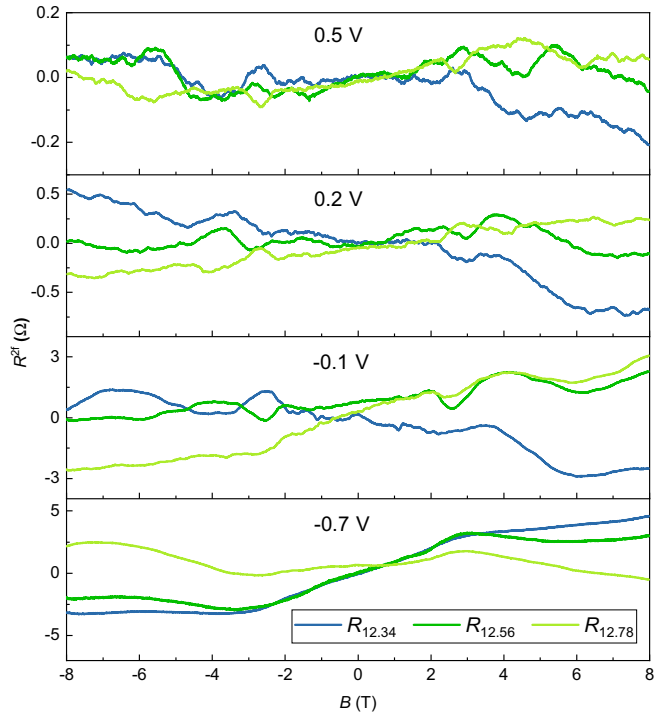


FIG. 2. In-plane magnetic field dependencies of $R^{2f}_{12,kl}(B)$ measured across three voltage contact pairs (as labeled in the legend) on the Hall bar device when $\theta = 0°$. The four panels are plotted for four different gate voltages, $V_g = 0.5$, 0.2, −0.1, and −0.7 V from top to bottom, respectively.

clearly visible in Fig. 2, where no general statement can be made about the symmetry of the $2f$ signals with respect to the B field.

For completeness, given that the key identifying signature of many effects [9–12,15,17,20] is an angular dependence of the nonlinear response, we explore such a possibility in Fig. 3. It presents $1f$ and $2f$ measurements of the $R_{12,46}$ and $R_{12,56}$ signals for magnetic field applied along various in-plane directions [see Fig. 1(a) for a graphical description of the angle θ], and gate voltage of 0.2 V. It is apparent that while each contact configuration produces signals that vary with the angle of the magnetic field, the signal is dominated by contribution from charge puddles, with extrema lining up regardless of an angle of the applied magnetic field. This of course would make identification of any other coexisting mechanism challenging.

III. CONCLUSIONS

With growing interest in studying complex nonlinear transport phenomena [8–20], the need for measurements of small nonlinear signals grew significantly in the recent years. Our findings highlight that, contrary to common perception, a careful study of such signals is not at all a trivial task. Not only must one conclusively rule out any nonlinearities originating from the measurement circuit or the sample contacts, but also those stemming from electronic transport in systems with charge puddles, which are ubiquitous to narrow gap materials. Given that the above produces harmonic distortions of

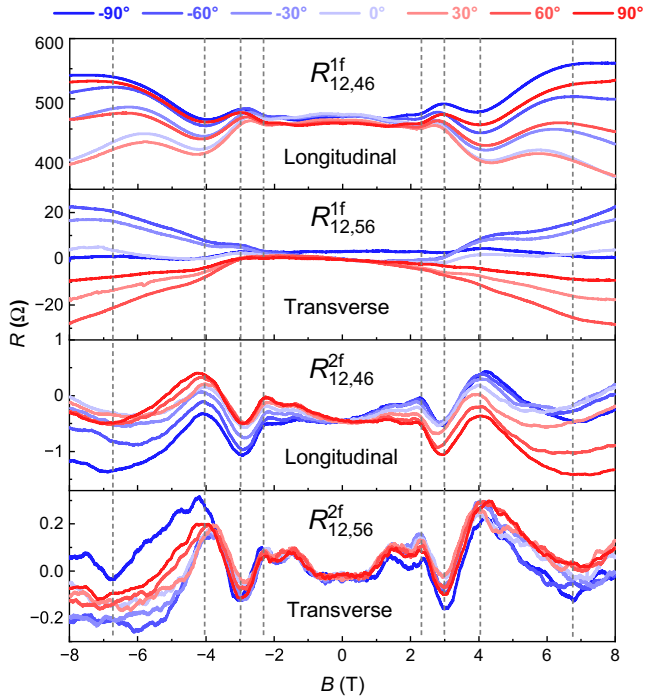


FIG. 3. $R^{1f}_{12,46}(B)$, $R^{1f}_{12,56}(B)$ (after subtraction of a linear contribution; see text for details), $R^{2f}_{12,46}(B)$, and $R^{2f}_{12,56}(B)$ measured as a function of the in-plane magnetic field when the in-plane angle θ is varied from -90° to 90° at a representative top-gate voltage $V_g = 0.2$ V. The vertical dashed lines are guides to the eye.

similar, or even greater magnitude than that typically predicted by nonlinear quantum effects, great caution is needed when analyzing such signals. In this context, even symmetry-based arguments that are often used to identify intrinsic nonlinear quantum responses may be unreliable, as the charge puddles not only induce nonlinearities arising from spatial inhomogeneities, but also arbitrarily mix longitudinal and transverse responses to an electric field, locally breaking the intrinsic bulk crystal symmetries.

It is also worth noting that, while narrow band-gap materials are especially prone to harmonic distortions due to charge puddles, artifact-free detection of subtle subpercent nonlinearities is extraordinarily challenging even in wide band-gap materials. The statement about great caution being needed when analyzing such signals applies generally to *any* nonlinear transport experiment.

ACKNOWLEDGMENTS

We thank L. Fu, Y. Zhang, T. Neupert, S. Tsirkin, I. Sodemann, W. Beugeling, and B. Trauzettel for useful discussions and L. Fürst and L. Lunczer for growing the HgTe epilayer. This work was supported by projects SFB 1170 (Project ID 258499086), and through the Würzburg-Dresden Cluster of Excellence on Complexity, Topology and Dynamics in Quantum Matter (EXC 2147, 390858490); by the Free State of Bavaria through the Institute for Topological Insulators and StMWi Project No. DB001905; and through a Max Planck fellowship at the Max Planck Institute for Chemical Physics of Solids, Dresden.

DATA AVAILABILITY

The data that support the findings of this article are openly available [37].

[1] M. V. Berry, Quantal phase factors accompanying adiabatic changes, Proc. R. Soc. A **392**, 45 (1984).
[2] D. Xiao, M.-C. Chang, and Q. Niu, Berry phase effects on electronic properties, Rev. Mod. Phys. **82**, 1959 (2010).
[3] D. J. Thouless, M. Kohmoto, M. P. Nightingale, and M. den Nijs, Quantized Hall conductance in a two-dimensional periodic potential, Phys. Rev. Lett. **49**, 405 (1982).
[4] N. Nagaosa, J. Sinova, S. Onoda, A. H. MacDonald, and N. P. Ong, Anomalous Hall effect, Rev. Mod. Phys. **82**, 1539 (2010).
[5] J. Sinova, S. O. Valenzuela, J. Wunderlich, C. H. Back, and T. Jungwi rth, Spin Hall effects, Rev. Mod. Phys. **87**, 1213 (2015).
[6] C.-Z. Chang, C.-X. Liu, and A. H. MacDonald, *Colloquium*: Quantum anomalous Hall effect, Rev. Mod. Phys. **95**, 011002 (2023).
[7] M. Z. Hasan and C. L. Kane, *Colloquium*: Topological insulators, Rev. Mod. Phys. **82**, 3045 (2010).
[8] I. Sodemann and L. Fu, Quantum nonlinear Hall effect induced by Berry curvature dipole in time-reversal invariant materials, Phys. Rev. Lett. **115**, 216806 (2015).
[9] K. Yasuda, A. Tsukazaki, R. Yoshimi, K. Kondou, K. S. Takahashi, Y. Otani, M. Kawasaki, and Y. Tokura, Current-nonlinear Hall effect and spin-orbit torque magnetization switching in a magnetic topological insulator, Phys. Rev. Lett. **119**, 137204 (2017).
[10] T. Ideue, K. Hamamoto, S. Koshikawa, M. Ezawa, S. Shimizu, Y. Kaneko, Y. Tokura, N. Nagaosa, and Y. Iwasa, Bulk rectification effect in a polar semiconductor, Nat. Phys. **13**, 578 (2017).
[11] Y. Tokura and N. Nagaosa, Nonreciprocal responses from non-centrosymmetric quantum materials, Nat. Commun. **9**, 3740 (2018).
[12] P. He, S. S.-L. Zhang, D. Zhu, Y. Liu, Y. Wang, J. Yu, G. Vignale, and H. Yang, Bilinear magnetoelectric resistance as a probe of three-dimensional spin texture in topological surface states, Nat. Phys. **14**, 495 (2018).
[13] Q. Ma, S.-Y. Xu, H. Shen, D. MacNeill, V. Fatemi, T.-R. Chang, A. M. Mier Valdivia, S. Wu, Z. Du, C.-H. Hsu, *et al.*, Observation of the nonlinear Hall effect under time-reversal-symmetric conditions, Nature (London) **565**, 337 (2019).
[14] K. Kang, T. Li, E. Sohn, J. Shan, and K. F. Mak, Nonlinear anomalous Hall effect in few-layer WTe_2, Nat. Mater. **18**, 324 (2019).
[15] P. He, S. S.-L. Zhang, D. Zhu, S. Shi, O. G. Heinonen, G. Vignale, and H. Yang, Nonlinear planar Hall effect, Phys. Rev. Lett. **123**, 016801 (2019).
[16] Z. Z. Du, H.-Z. Lu, and X. C. Xie, Nonlinear Hall effects, Nat. Rev. Phys. **3**, 744 (2021).

[17] W. Rao, Y.-L. Zhou, Y.-j. Wu, H.-J. Duan, M.-X. Deng, and R.-Q. Wang, Theory for linear and nonlinear planar Hall effect in topological insulator thin films, Phys. Rev. B **103**, 155415 (2021).

[18] P. He, G. K. W. Koon, H. Isobe, J. Y. Tan, J. Hu, A. H. Castro Neto, L. Fu, and H. Yang, Graphene moiré superlattices with giant quantum nonlinearity of chiral Bloch electrons, Nat. Nanotechnol. **17**, 378 (2022).

[19] H. F. Legg, M. Rößler, F. Münning, D. Fan, O. Breunig, A. Bliesener, G. Lippertz, A. Uday, A. A. Taskin, D. Loss, J. Klinovaja, and Y. Ando, Giant magnetochiral anisotropy from quantum-confined surface states of topological insulator nanowires, Nat. Nanotechnol. **17**, 696 (2022).

[20] M. Suárez-Rodríguez, F. de Juan, I. Souza, M. Gobbi, F. Casanova, and L. E. Hueso, Nonlinear transport in non-centrosymmetric systems, Nat. Mater. **24**, 1005 (2025).

[21] H. Beidenkopf, P. Roushan, J. Seo, L. Gorman, I. Drozdov, Y. S. Hor, R. J. Cava, and A. Yazdani, Spatial fluctuations of helical Dirac fermions on the surface of topological insulators, Nat. Phys. **7**, 939 (2011).

[22] B. Skinner, T. Chen, and B. I. Shklovskii, Why is the bulk resistivity of topological insulators so small? Phys. Rev. Lett. **109**, 176801 (2012).

[23] M. König, M. Baenninger, Andrei G. F. Garcia, N. Harjee, B. L. Pruitt, C. Ames, P. Leubner, C. Brüne, H. Buhmann, L. W. Molenkamp, and Gordon D. Goldhaber, Spatially resolved study of backscattering in the quantum spin Hall state, Phys. Rev. X **3**, 021003 (2013).

[24] D. Nandi, B. Skinner, G. H. Lee, K.-F. Huang, K. Shain, C.-Z. Chang, Y. Ou, S.-P. Lee, J. Ward, J. S. Moodera, P. Kim, B. I. Halperin, and A. Yacoby, Signatures of long-range-correlated disorder in the magnetotransport of ultrathin topological insulators, Phys. Rev. B **98**, 214203 (2018).

[25] A. Thenapparambil, G. E. Dos Santos, C.-A. Li, M. Abdelghany, W. Beugeling, H. Buhmann, C. Gould, S.-B. Zhang, B. Trauzettel, and L. W. Molenkamp, Fluctuations in planar magnetotransport due to tilted Dirac cones in topological materials, Nano Lett. **23**, 6914 (2023).

[26] S.-H. Zheng, H.-J. Duan, J.-K. Wang, J.-Y. Li, M.-X. Deng, and R.-Q. Wang, Origin of planar Hall effect on the surface of topological insulators: Tilt of Dirac cone by an in-plane magnetic field, Phys. Rev. B **101**, 041408(R) (2020).

[27] P. Leubner, L. Lunczer, C. Brüne, H. Buhmann, and L. W. Molenkamp, Strain engineering of the band gap of HgTe quantum wells using superlattice virtual substrates, Phys. Rev. Lett. **117**, 086403 (2016).

[28] J. Ruan, S.-K. Jian, H. Yao, H. Zhang, S.-C. Zhang, and D. Xing, Symmetry-protected ideal Weyl semimetal in HgTe-class materials, Nat. Commun. **7**, 11136 (2016).

[29] D. M. Mahler, J.-B. Mayer, P. Leubner, L. Lunczer, D. Di Sante, G. Sangiovanni, R. Thomale, E. M. Hankiewicz, H. Buhmann, C. Gould, and L. W. Molenkamp, Interplay of Dirac Nodes and Volkov-Pankratov Surface States in Compressively Strained HgTe, Phys. Rev. X **9**, 031034 (2019).

[30] K. Bendias, S. Shamim, O. Herrmann, A. Budewitz, P. Shekhar, P. Leubner, J. Kleinlein, E. Bocquillon, H. Buhmann, and L. W. Molenkamp, High mobility HgTe microstructures for quantum spin Hall studies, Nano Lett. **18**, 4831 (2018).

[31] P. Shekhar, S. Shamim, S. Hartinger, R. Schlereth, V. Hock, H. Buhmann, J. Kleinlein, and L. W. Molenkamp, Low-temperature atomic layer deposition of hafnium oxide for gating applications, ACS Appl. Mater. Interfaces **14**, 33960 (2022).

[32] See Supplemental Material at http://link.aps.org/supplemental/10.1103/mc1p-blhk for a detailed overview of the second harmonic measurement setup and additional experimental data, which also includes Refs. [33,34].

[33] NF Corporation, 3625 dual channel programmable filter: Instruction manual, revision 1.0 ed. (NF Corporation, 2012), https://www.nfcorp.co.jp/english/sup/download/manual/mi/pdf/e_3625.pdf.

[34] Stanford Research Systems, DS360 ultra low distortion function generator: Operating manual and programming reference, revision 2.9 ed. (Stanford Research Systems, 2021), https://www.thinksrs.com/downloads/pdfs/manuals/DS360m.pdf.

[35] S.-B. Zhang, C.-A. Li, F. Pena-Benitez, P. Surowka, R. Moessner, L. W. Molenkamp, and B. Trauzettel, Super-resonant transport of topological surface states subjected to in-plane magnetic fields, Phys. Rev. Lett. **127**, 076601 (2021).

[36] J. Arrillaga and N. R. Watson, Subject definition and objectives, in *Power System Harmonics,* 2nd ed. (Wiley, Chichester, UK, 2004), Chap. 1, pp. 1–18.

[37] A. Thenapparambil, K. M. Fijalkowski, M. AbdelGhany, H. Buhmann, C. Gould, and L. W. Molenkamp, Data for Thenapparambil A. et al. "Charge puddles complicate nonlinear transport in large Berry phase materials", Zenodo (2026), 10.5281/zenodo.18554519.